Correspondence

Transducer for Harmonic Intravascular Ultrasound Imaging

Hendrik J. Vos, Martijn E. Frijlink, Erik Droog, David E. Goertz, Gerrit Blacquière, Anton Gisolf, Nico de Jong, *Associate Member, IEEE*, and Antonius F. W. van der Steen, *Member, IEEE*

***Abstract*—A recent study has shown the feasibility of tissue harmonic imaging (THI) using an intravascular ultrasound (IVUS) transducer. This correspondence describes the design, fabrication, and characterization of a THI-optimized piezoelectric transducer with oval aperture of 0.75 mm by 1 mm. The transducer operated at 20 MHz and 40 MHz, and was comprised of a single piezoelectric layer with additional passive layers. The Krimholtz-Leedom-Matthaei (KLM) model was used to iteratively find optimal material properties of the different layers. The transducer characterization showed −6 dB fractional bandwidths of 30% and 25%, and two-way insertion losses of −20 dB and −36 dB, respectively.**

I. Introduction

In clinical investigation of atherosclerosis, intravascular ultrasound (IVUS) catheters are used for imaging the arterial wall [1]. They form images with either fast-rotating single element transducers or with array configurations. Current IVUS catheters operate in linear imaging mode, and they can suffer from limitations such as ring-down, side-lobes in the ultrasound beam and reflections from the protecting catheter sheath, which reduce the image quality. From conventional cardiovascular imaging, it is known that many of these effects may be reduced with tissue harmonic imaging (THI), in which nonlinear propagation distorts the fundamental frequency pressure pulse, thereby generating higher harmonics [2]. The generation of a second harmonic signal is approximately proportional to the square of the local fundamental frequency pressure at moderate pressures [2]. Less harmonic energy is present close to the transducer at which the artifacts occur mostly [3]. This beneficial effect comes at the cost of lower signal levels of the harmonics, which can be overcome by carefully designing the transducer for harmonic imaging [4], [5].

Initial studies have shown the feasibility of THI in IVUS imaging [6], [7], but these were carried out with transducers that were not optimized for THI. Various fundamental and harmonic imaging transducers for diagnostic medical high-frequency ultrasound are described in the literature [3], [8]–[10], mostly based on PVDF and lithium niobate. However, compared to PZT ceramics, these materials have a low dielectric constant, which results in a bad electric match to conventional 50 ohm electronics if the element size is small. Reported IVUS transducers [11]–[13] have not been optimized for harmonic imaging. Therefore, a new PZT-based single element IVUS transducer is developed with dual frequency band sensitivity of about 20 MHz and 40 MHz.

Manuscript received November 2, 2004; accepted May 25, 2005. The Dutch Technology Foundation STW financially supports this work (Project RPG 5442).

H. J. Vos, M. E. Frijlink, E. Droog, D. E. Goertz, N. de Jong, and A. F. W. van der Steen are with Biomedical Engineering, Thoraxcenter, Erasmus Medical Center, Rotterdam, The Netherlands (e-mail: A.VanderSteen@ErasmusMC.nl).

H. J. Vos, E. Droog, and A. Gisolf are with the Delft University of Technology, Delft, The Netherlands.

E. Droog and G. Blacquière are with TNO-TPD, Delft, The Netherlands.

D. E. Goertz, N. De Jong, and A. F. W. van der Steen are also with Interuniversity Cardiology Institute of The Netherlands.

N. De Jong is also with the University of Twente, Twente, The Netherlands.

II. Methods and Fabrication

A. Design

The purpose of the transducer imposes several design constraints. The center frequency of the transmission pulse was chosen to be 20 MHz, resulting in a second harmonic pulse with a center frequency of 40 MHz. These frequencies are thought to give a good trade-off between axial resolution (which increases with frequency) and penetration depth (which reduces with frequency due to increased acoustic attenuation). As the transducer is mounted inside a catheter tip with 1.3 mm outer diameter (4 Fr), the aperture should not exceed 0.75 mm by 1.0 mm. The matching layers should be electrically conductive to facilitate connection of the electrodes.

Based on these constraints, a design was made consisting of a single disc of piezoelectric material and two passive layers for frequency tuning and improved acoustic impedance matching (Fig. 1). An additional passive layer is sandwiched between the sound-absorbing backing material and the piezoelectric layer and acts as a so-called mismatching layer [14], increasing the power transmission efficiency in the forward direction.

The transducer was modeled with the one-dimensional KLM model, which was extended with acoustic and electric energy loss [11], [15]–[17]. In order to optimize the transducer for harmonic imaging, a multidimensional, nonlinear minimization algorithm (Nelder-Mead simplex method) was implemented. Basically this minimization algorithm searches for the thickness of the active layer and the thickness and acoustical impedances of the passive layers that maximize the transmission efficiency and the reception sensitivity.

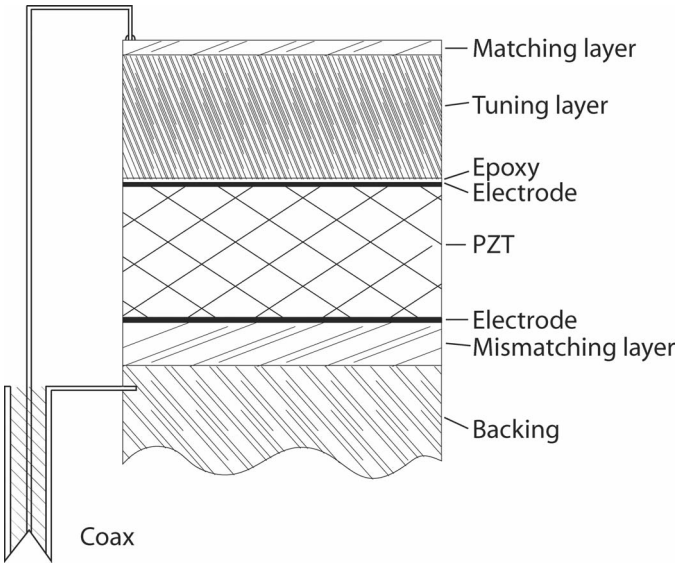

Fig. 1. Schematic of the transducer. All passive layers are electrically conductive for easy connection. The transducer is oval shaped with axes of 0.75 mm and 1.0 mm.

This search was associated with the following cost function:

$$\chi = -\log\left\{T_f^2\left(f_0\right)\right\} - \log\left\{T_f^{-1}\left(2f_0\right)\right\}, \qquad (1)$$

with T_f the ratio of the output acoustic force and the source voltage, T_f^{-1} its reception inverse and f_0 the fundamental frequency (20 MHz). We assumed that the maximum allowed transmission voltage is limited by health care regulations; and, due to the squared dependency of the harmonic pressure generation on the fundamental pressure, the cost function relies on the squared transmission function. Logarithms were used for faster convergence.

Material properties of fine-grain, high-pressed PZT (PPK22, Stelco GmbH, Neumarkt, Germany) were inserted in the model. This material was chosen for its low loss at high frequencies (mechanic loss factor of 0.02 and electric loss factor of 0.03 at 20 MHz), and has a thickness mode coupling coefficient of 0.42 and a relative clamped dielectric constant of 850.

Based on the available electrically conductive materials (see Section III-B), the acoustic impedance of the backing was set to 7 MRayl and the acoustic impedance of the mismatching layer was set to 4 MRayl.

The optimized layer properties based on the extended KLM model are given in Table I. The optimal transducer surface is 1.1 mm^2, but the size restrictions of the element resulted in a maximum area of 0.6 mm^2 (elliptical aperture with 0.75 mm and 1.0 mm axes). Simulations showed that this aperture reduction increases the two-way insertion loss with less than 2 dB. The depicted sound velocities and loss factors are measured values of the available materials, on which the prototype is based (see Section III-B).

TABLE I
OPTIMAL SIMULATED VALUES OF MATERIAL PROPERTIES.[1]

Layer	Thickness (μm)	Velocity (m/s)	Z (MRayl)	Loss factor (−)
Matching layer	11 (7)	1500 *	4 (4)	0.05 *
Tuning layer	64 (59)	6400 *	27 (22)	0.01 *
Piezoelectric layer	71 (67)	5000 *	40 *	0.02 *
Mismatching layer	14 (21)	1500 *	4 *	0.05 *

[1]Asterisked numbers were manually inserted in the model and kept fixed during the optimization. The optimal values for the design including an adhesive film are depicted between parentheses.

B. Transducer Fabrication

A 0.5 mm thick disk of PZT was manually lapped and polished to the appropriate thickness and electroded with a 100 nm nickel film. The tuning layer was made from an aluminum foil (measured impedance of 17 MRayl), rolled to the appropriate thickness and bonded with two-component epoxy (AY103 and HY951, Ciba Specialty Chemicals, Basel, Switzerland) under pressure on the front side of the PZT layer. The thickness of the epoxy layer was estimated to be 0.5 μm, based on the assumption that the surface roughness of the polished and electroded PZT limits the epoxy layer thickness. It is hypothesized that the peaks of the nickel electrode penetrate through the epoxy layer to make contact with the aluminum layer, thus maintaining electric conductivity. The surface roughness was measured with a 0.1-μm resolution surface roughness instrument (Mitutoyo SJ-301, Mitutoyo American Corporation, Aurora, IL), and showed peak-to-peak values of about 1 μ. The layer thickness is estimated at half the peak-to-peak distance, because we expect half the interstitial volume filled with the PZT and half the volume filled with the epoxy.

Simulations indicated that the epoxy layer changes the optimal values for the layer properties; the new values are given between parentheses in Table I. The matching layer and the mismatching layer consisted of 45–55% mass percentage mixed silver- and carbon-filled conductive ink (SS477 RFU and SS427, Acheson Industries, Erstein, France) and had a measured acoustic impedance of 5 MRayl. The backing consisted of silver-filled, electrically conductive epoxy (EccoBond 66C, Emerson and Cuming, Westerlo, Belgium), which has an acoustic impedance of 7 MRayl.

Multiple prototype elements were laser-cut into ovals with axes of 1.0 mm and 0.75 mm and mounted on a catheter tip. For the characterization experiments, this tip was attached to a steel tube with an outer diameter of 0.9 mm. Both sides of the transducer were connected to the coaxial cable (Pico-coax PCX 44 K 11, Grandwill Axon, China), and the element was poled with an electric field of 25 kV/cm at room temperature.

C. Characterization

The electric impedance of the transducer in air was measured with a vector impedance analyzer (HP 4193A, Hewlett-Packard, Palo Alto, CA) before the cable was attached. The fabricated transducer material values were checked with the use of a curve-based fit of the KLM model implementation to the measured electric impedance in air, in which the sum of squared differences between the measured and modeled impedances was minimized. The Nelder-Mead simplex method was used to vary the input parameters. The layer properties thickness, acoustic impedance, and loss factor, together with the piezoelectric coupling factor and a serial loss resistance, were updated. Based on the found fit, the expected transfer function and two-way insertion loss of the transducer in water were calculated with the model.

The pressure transfer function of the transducer was measured using a hydrophone. The transducer was driven by a 10 V, single peak amplitude signal using an arbitrary waveform generator (AWG) (520 Tektronix, Portland, OR) in combination with a linear power amplifier (LPI-10 ENI, Rochester, NY). To improve the signal-to-noise ratio (SNR) for the frequency range of interest (10 MHz to 50 MHz), three separate 100% fractional bandwidth, Gaussian-enveloped pulses with center frequencies of 20 MHz, 30 MHz, and 40 MHz were applied. A needle-type hydrophone (0.075 mm diameter PVDF, Precision Acoustics, Dorchester, UK) was placed on-axis at 4.0 mm distance from the transducer, which is the theoretical natural focal distance at 40 MHz. The received signal was sampled by an 8-bit digitizer (DP235, Acqiris, Geneva, Switzerland) at 400 MHz and averaged over 400 pulses. The pressure transmission transfer function was calculated by the ratio of the hydrophone received spectrum, and the AWG driving spectrum and was compensated for by the calibrated hydrophone sensitivity characteristics. For efficiency measurements in a pulse-echo configuration, the signals were redirected with a passive diode expander/limiter with a two-way signal loss of 12 dB, for which compensation was performed. A flat stainless steel reflector was placed at 3.3 mm distance parallel to the transducer surface. The transmission pulses were similar to those in the hydrophone measurements and had a 5 V single peak amplitude. The received pulse was averaged over 1000 repetitions. The two-way insertion loss was calculated by the ratio of the received signal spectrum and the amplifier signal spectrum.

The measured transfer function and insertion loss were compared with the simulated functions of the modeled transducer with optimized values and with those resulting from the curve-based fit to the electric impedance. To account for the diffraction effects and water attenuation in the model, we used a numerical approach based on the Rayleigh-Sommerfeld integral [16] to calculate the spatial impulse response of the transmitter/receiver setup. In this method, the integral is approximated by a sum over small ($< 1/100\ \lambda^2$) surface elements on both the transmitting and receiving flat surfaces, and the received pressure is the average over the small elements of the receiving plane. The acoustic damping in water is 25 10^{-3} Np MHz^{-2} m^{-1} in water at 20°C [18], for which compensation was performed in the simulations.

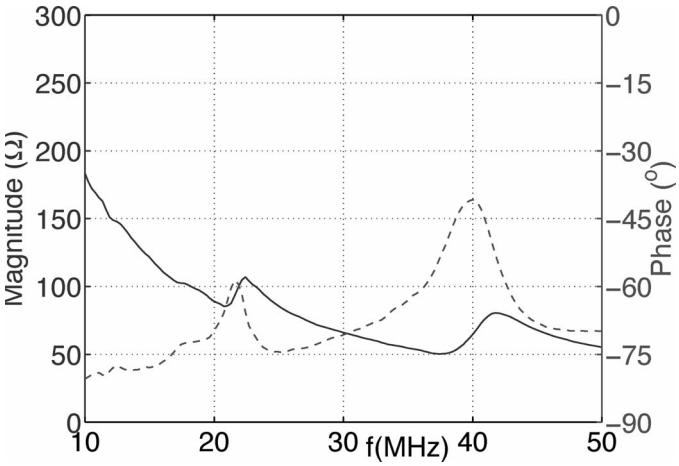

Fig. 2. Magnitude (solid) and phase (dashed) of the measured electric impedance of the transducer in air.

III. Results

Fig. 2 shows the measured electrical impedance of the element in air. The values found with the curve-based fit showed deviations smaller than 20% of the values from Table I. The passive electric loss resistance was 16 ohm, which was mainly caused by the relatively low electrical conductivity of the mixed silver and carbon layers (about 5 ohm per layer). The phase plot shows a peak at 22 MHz and 40 MHz. The fact that the lower-frequency peak is not exactly at 20 MHz is attributed to uncertainties associated with the modeling of the epoxy layer between the PZT and the aluminum layer.

Fig. 3 shows the measured and modeled transfer functions of the transducer at 4.0 mm. It is a graph composed from the three different pulses as described before, plotted in bins with ranges of 10–25 MHz, 25–35 MHz, and 35–50 MHz.

The transmission transfer function again shows peaks at 22 MHz and at 40 MHz, with −6 dB fractional bandwidths (BW) of 30% and 25%, respectively. The agreement of the modeled transfer function based on the curve-based fit and the measured transfer function is very good. However, the curve-based calculated pressure is lower than the modeled optimized transducer pressure, which we hypothesize to be due to two factors. First, simulations showed that the epoxy layer can cause unwanted reverberations between layers as it becomes thicker. This resulted in a reduction of 3 dB of the transmit efficiency for the specified bonding layer. Second, the other factor might be the electric resistance of the transducer, causing heat production, which resulted in 2 dB energy loss in simulations. The modeled

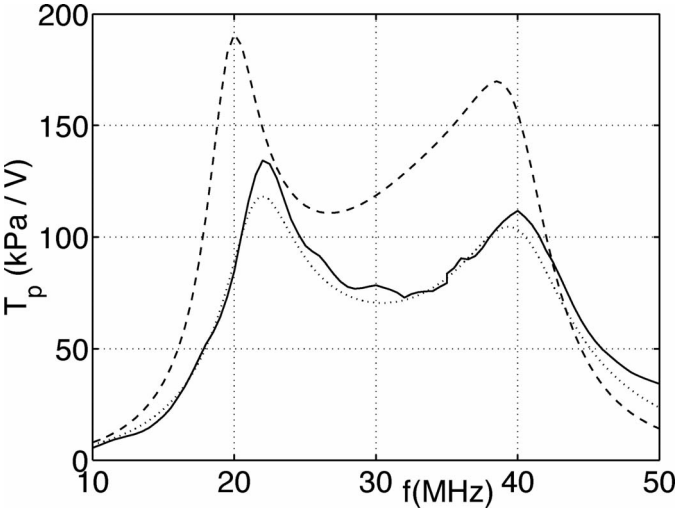

Fig. 3. Measured (solid) and modeled (dotted) transfer function of the transducer at 4.0 mm distance in water. The dashed line shows the modeled transfer function of the optimized transducer. Water attenuation and diffraction are incorporated in the modeled functions.

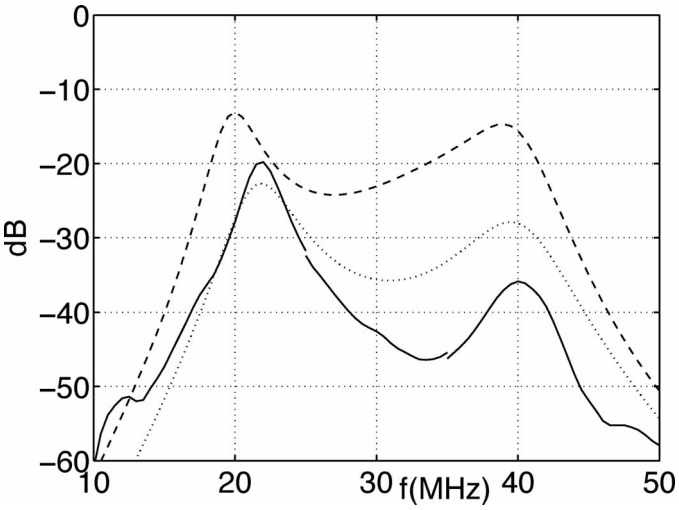

Fig. 4. Measured (solid) and modeled (dotted) two-way insertion loss of the element, with a flat steel reflector at 3.3 mm distance. The dashed line shows the optimized transducer round trip insertion loss. Water attenuation and diffraction are incorporated in the modeled functions.

optimized transducer showed 40% and 35% BW of about 20 MHz and 40 MHz, respectively.

Fig. 4 shows the measured and modeled two-way insertion loss of the transducer. The modeled insertion loss from the curve-based fit and the measured one show good agreement up to 25 MHz and an increasing difference between 25 and 45 MHz of up to 12 dB. Again, the epoxy layer (6 dB, two-way loss) and the loss resistance (4 dB, two-way loss) are hypothesized to give the differences between the optimized simulated design and the calculated insertion loss based on the curve-based fit. Additionally, in the measurements, a suboptimal alignment of the reflector might give undesired diffraction effects, which are absent in the beam profile simulations. Electric tuning effects due to the expander/limiter also might give reverberations, resulting in frequency-dependent interference attributed to the measured insertion loss. Unfortunately, we are not able to quantify these influences, but we only can suspect them to give the differences between the model based on the electrical impedance fit and the measured two-way insertion loss.

IV. Conclusions

An ultrasound transducer optimized for harmonic IVUS has been designed, built, and characterized. The modeled optimized properties of the transducer layers were found with an extended version of the KLM model combined with a nonlinear minimization algorithm. The prototype showed a −6 dB fractional bandwidth of about 20 MHz of 30%, which should be sufficient for a short pulse. The most efficient transmit frequency of the current prototype appeared to be 22 MHz instead of 20 MHz. This frequency could be tuned in future transducers to 20 MHz by increasing the thickness of the aluminum layer in the design.

The mismatching and the matching layers are the main causes of electrical energy loss, reducing the efficiency and increasing the risk of transducer overheating in a catheter setup. Using a backing material with lower acoustic impedance, which would eliminate the need for a mismatching layer, could alleviate this problem. This material also could be used for the front matching layer.

The surface area of the prototype is smaller than the most optimal surface area, resulting in an electric mismatch between the transducer and the electrical equipment. However, additional simulations showed that this gave a two-way insertion loss increase of about 2 dB, which is negligible compared to the losses described above.

Acknowledgment

We would like to thank Gerrit van Dijk for his major contribution to the fabrication of the transducer. This project is supported by an NWO-STW Pioneer grant RPG-5442.

References

[1] Y. Saijo and A. F. W. van der Steen, Eds. *Vascular Ultrasound*. Tokyo: Springer-Verlag, 2003.

[2] F. A. Duck, "Nonlinear acoustics in diagnostic ultrasound," *Ultrasound Med. Biol.*, vol. 28, no. 1, pp. 1–18, 2002.

[3] E. W. Cherin, J. K. Poulsen, A. F. W. van der Steen, P. Lum, and F. S. Foster, "Experimental characterization of fundamental and second harmonic beams for a high-frequency ultrasound transducer," *Ultrasound Med. Biol.*, vol. 28, no. 5, pp. 635–646, 2002.

[4] S. Saitoh, M. Izumi, and Y. Mine, "A dual frequency ultrasonic probe for medical applications," *IEEE Trans. Ultrason., Ferroelect., Freq. Contr.*, vol. 42, no. 2, pp. 294–300, 1995.

[5] S. Takeuchi, M. R. A. A. Zaabi, T. Sato, and N. Kawashima, "Ultrasound transducer with double-peak frequency characteristics for subharmonic imaging," *Jpn. J. Appl. Phys.*, vol. 42, no. 1-5B, pp. 3253–3254, 2003.

[6] A. F. W. van der Steen, J. K. Poulsen, E. Cherin, and F. S. Foster, "Harmonic imaging at high frequencies for IVUS," in *Proc. IEEE Ultrason. Symp.*, 1999, pp. 1537–1540.

[7] M. E. Frijlink, D. E. Goertz, L. C. A. van Damme, R. Krams, and A. F. W. van der Steen, "Intravascular ultrasound tissue harmonic imaging in vivo," in *Proc. IEEE Ultrason. Symp.*, 2004, pp. 1118–1121, to be published.

[8] A. Fleischmann, R. Modi, A. Nair, J. Talman, G. Lockwood, and S. Roy, "Miniature high frequency focused ultrasonic transducers for minimally invasive imaging procedures," *Sens. Actuators A*, vol. 103, pp. 76–82, 2003.

[9] Q. F. Zhou, J. Cannata, C. Z. Huang, H. K. Guo, V. Marmarelis, and K. K. Shung, "Fabrication and modeling of inversion layer ultrasonic transducers using $LiNbO_3$ single crystal," in *Proc. IEEE Ultrason. Symp.*, 2003, pp. 1034–1037.

[10] R. J. Meyer, S. Alkoy, R. Newnham, and J. Cochran, "Development of materials and composites for >25 MHz single element transducers," in *Proc. IEEE Ultrason. Symp.*, 1999, pp. 1299–1302.

[11] F. S. Foster, L. K. Ryan, and D. H. Turnbull, "Characterization of lead zirconate titanate ceramics for use in miniature high-frequency (20–80 MHz) transducers," *IEEE Trans. Ultrason., Ferroelect., Freq. Contr.*, vol. 38, no. 5, pp. 446–453, 1991.

[12] O. Oralkan, A. S. Ergun, J. A. Johnson, M. Karaman, U. Dernirci, K. Kaviani, T. H. Lee, and B. T. Khuri-Yakub, "Capacitive micromachined ultrasonic transducers: Next generation arrays for acoustic imaging?," *IEEE Trans. Ultrason., Ferroelect., Freq. Contr.*, vol. 49, no. 11, pp. 1596–1610, 2002.

[13] J. G. Knight and F. L. Degertekin, "Fabrication and characterization of cMUTs for forward looking intravascular ultrasound imaging," in *Proc. IEEE Ultrason. Symp.*, 2003, pp. 577–580.

[14] J. Souquet, P. Defranould, and J. Desbois, "Design of low-loss wide-band ultrasonic transducers for noninvasive medical applications," *IEEE Trans. Sonics Ultrason.*, vol. SU-26, no. 2, pp. 75–81, 1979.

[15] M. Lethiecq, L. P. Tran-Huu-Hue, F. Patat, and L. Pourcelot, "Measurement of losses in five piezoelectric ceramics between 2 and 50 MHz," *IEEE Trans. Ultrason., Ferroelect., Freq. Contr.*, vol. 40, no. 3, pp. 232–237, 1993.

[16] G. S. Kino, *Acoustic Waves: Devices, Imaging and Analog Signal Processing*. Englewood Cliffs, NJ: Prentice-Hall, 1987, pp. 27–74.

[17] R. Krimholtz, D. A. Leidom, and G. L. Matthaei, "New equivalent circuits for elementary piezoelectric transducers," *Electron. Lett.*, vol. 6, no. 13, pp. 389–399, 1970.

[18] F. A. Duck, *Physical Properties of Tissue*. New York: Academic, 1990, pp. 73–96.